RSC Advances

ROYAL SOCIETY OF CHEMISTRY

www.rsc.org/advances

Air-processed, efficient $CH_3NH_3PbI_{3-x}Cl_x$ perovskite solar cells with organic polymer PTB7 as a hole-transport layer

Yangyang Du, Hongkui Cai *, Jian Ni, Juan Li, Hailong, Yu, Xiaoxiang Sun, Yuxiang Wu, Hongbin Wen, Jianjun Zhang*

College of Electronic Information and Optical Engineering, Nankai University, Tianjin, 300071, China

ABSTRACT:

Low-temperature, solution-processed perovskite solar cells (PSCs), which utilized organic poly[4,8-bis[(2-ethylhexyl)oxy]benzo[1,2-b:4,5-b']dithiophene-2,6-diyl][3-fluoro-2-[(2-ethylhexyl)carbonyl]thieno[3,4-b]-thiophenediyl] (PTB7) as a hole-transport layer (HTL), achieved a power conversion efficiency (PCE) as high as 13.29% when fabricated in ambient air. Through a comparative study, we demonstrate this PCE value to be superior compared to its counterparts with Spiro-OMeTAD or P3HT as the HTL; the superiority consists in higher fill factor (FF) and open-circuit voltage (V_{oc}). By probing the absorption spectrum of $CH_3NH_3PbI_{3-x}Cl_x$ before and after spin-coating the PTB7, it is discovered that the spin coating of PTB7 has little influence on the quality of the perovskite films. Furthermore, it is shown that PTB7 possesses higher conductivity compared with conventional HTLs, including Spiro-OMeTAD, P3HT and PCDTBT. Moreover, in order to further improve device performance, the prevalent additives lithium bis (trifluoromethylsulphony) imide (LiTFSI) and 4-tert-butylpyridine (t-Bp) are investigated, along with a post-annealing process that is applied to the whole device. The results presented here and the overall fabrication method represent a helpful new approach for fabricating highly efficient perovskite -based photovoltaic devices.

KEYWORDS: Perovskite solar cells (PSCs); PTB7; ambient air; conductivity.

*Corresponding author: caihongkun@nankai.edu.cn (H. Cai)

*Corresponding author: jjzhang@nankai.edu.cn (J. Zhang)

Tel: +8602223508046

1. Introduction

Organic-inorganic hybrid perovskite solar cells (PSCs) have attracted increased attention recently, and

are considered to be a future candidate in the field of solar cells on account of their distinct merits, which include low-cost, large photon absorption coefficients, long charge carrier diffusion, etc. [1-5]. The hybrid materials $CH_3NH_3PbI_3$ and $CH_3NH_3PbBr_3$ initially derived from dye-sensitized solar cell (DSSC) acting as sensitizer [1, 5]. However, their power conversion energy (PCE) is rather poor, and their stability is similarly poor. That is because these materials severely decompose when exposed to liquid electrolytes, which limits their PCE to 6.5% [5].

Subsequently, all solid-state perovskite solar cells with PCEs of 10% were reported in 2012 by replacing the liquid electrolyte with solid Spiro-OMeTAD [3, 6]. As a result, PCE values over 15% were obtained in PSCs with mesoporous architecture, as well as planar heterojunction architecture [7-9]. Surprisingly, the measured PCE dramatically surged, exceeding 20.1% in the past year [10]. So far, the study of PSCs has witnessed remarkable breakthroughs, including interface engineering [11, 12], diverse preparation methods regarding perovskite absorbers [2, 7, 13, 14], illustrating the effect of moisture on the growth of perovskite films [15, 16], the design of cell construction [3, 4, 6, 8], etc.. Moreover, flexible PSCs with PCEs over 10% were also reported this year [17].

However, in the reported high-efficiency PSCs, the HTL was mainly limited to organic compounds such as Spiro-OMeTAD, which are costly and require complex doping and long oxidation time [3,16,18]. Furthermore, the device fabrication was mainly carried out in glove- boxes filled with nitrogen, which significantly hinders the further development and practical application of these devices. Accordingly, researchers have made great efforts to explore alternative HTLs for use in PSCs. In particular, diverse p-type polymeric organic semiconductors were investigated as HTLs, including PCDTBT, P3HT, PCPDTBT, PTAA, etc. [18-22]. Nevertheless, some studies have demonstrated that when P3HT and PCPDTBT are deposited on the perovskite, the perovskite quality of crystallization decreases, which leads to severe carrier recombination, and weakens the performance of the device [18]. At the same time, using PTAA as a HTL can lead to a higher open-circuit voltage (V_{oc}) and a higher fill factor (FF) as compared with the devices that use Spiro-OMeTAD (under the same conditions) , and can furthermore achieve a PCE of 17.2% [18]. In addition, some small molecules [20] and inorganic HTLs [23] have

been used in PSCs, which implies that Spiro-OMeTAD may be not the best choice for achieving highly efficient PSCs.

Hence, the organic polymer PTB7 is employed as the HTL in PSCs in this study. The device was fabricated according to the following construction: FTO / compact TiO_2 (c-TiO_2) / mesoporous TiO_2 (m-TiO_2) / $CH_3NH_3PbI_{3-x}Cl_x$ / PTB7 / silver (see Figure 1.a and b). PTB7 was adopted as the HTL of PSCs because of the following reasons. First of all, the highest occupied molecular orbital (HOMO) energy level of PTB7 (as determined by photoelectron spectroscopy) is found to be 5.2 eV, which is higher than that of $CH_3NH_3PbI_{3-x}Cl_x$ (Figure 1.c); this, ensures efficient extraction of holes from $CH_3NH_3PbI_{3-x}Cl_x$ to PTB7, and subsequently to the silver counter electrode. The energy level alignment of TiO_2, $CH_3NH_3PbI_{3-x}Cl_x$, and various HTLs (such as PTB7, P3HT, etc.) are presented in Figure 1.c, which implies PTB7 possess suitable energy match with $CH_3NH_3PbI_{3-x}Cl_x$ to extract holes and block electrons. Secondly, the conductivity of PTB7 is an order of magnitude higher than that of spiro-OMeTAD, P3HT, etc., which was demonstrated by the test of Photo-Dark Conductivity summarized in Table 2. Thirdly, the process of spin - coating PTB7 can maintain the quality of perovskite films, which is crucial to effective photoelectric conversion. Consequently, the confluence of excellent conductivity with suitable energy match makes it an impressive HTL candidate in perovskite- based photovoltaics.

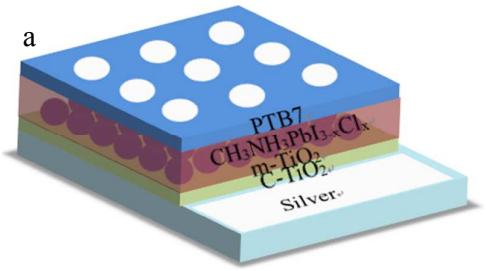

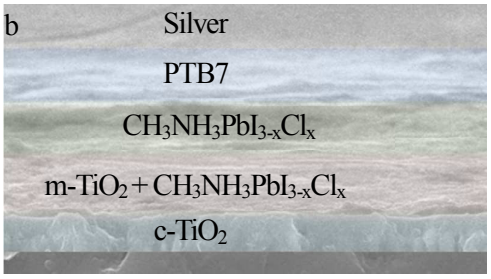

Figure 1 (a) device structure diagram of the FTO / c-TiO2 / m-TiO2 / $CH_3NH_3PbI_{3-x}Cl_x$ / PTB7 / Spiro-OMeTAD / P3HT / PCDTBT / Silver; (b) the cross-section SEM image of the whole device; (c) corresponding energy level alignment of the device.

2. Experimental

2.1. Measurements

The surface morphologies of the $CH_3NH_3PbI_{3-x}Cl_x$ film were observed by scanning electron microscope (SEM) (Hitachi SU8010) and atomic force microscopy (AFM) (Seiko SPA-400 SPM UNIT). The X-ray diffraction（XRD）(Philips PANalytical X'Pert Pro, Cu Kα）was used to determine the crystal structure and phase of $CH_3NH_3PbI_{3-x}Cl_x$ film. The transmittance and absorption spectra of films were measured by a UV-VIS spectrophotometer (Cary 5000). The electrical conductivity was measured by Photo-Dark Conductivity (PDC-40A). The current density-voltage (J-V) characteristics of the devices were measured with a Abet sun 2000 solar simulator under the illumination of an AM 1.5G (100 mW/cm^2).

2.2. Compact hole blocking layer (c-TiO2)

The precursors of compact titanium dioxide were prepared by adding 5 mL of tetrabutyl titanate to 25 mL of ethanol, followed by 0.2 g of polyethylene glycol, 1 mL of nitric acid, and 0.5 mL of deionized water. Next, we stirred the mixed solution for 5 h and then let it rest still for 15 h in order to ensure that the precipitate sunk. (The upper clear solution was desired substance.) The blocking layer was formed by spin coating the prepared suspension onto FTO glasses at 2500 rpm for 40s, followed by annealing at 120 ℃ for 5 min, and annealing at 500 ℃ for 30 min .

2.3. Mesoporous nanoparticles

The anatase-titania nanoparticles were mixed with ethanol. The mixture was then stirred with a magnetic

stirrer at room temperature for 30 min. Next, terpineol and ethylcellulose were added to the above mixture, and the mixture was stirred for 90 min at 200 rpm until the titanium dioxide slurry was obtained. The mass ratio of ethylcellulose to anatase-titania nanoparticles was 1:2, whereas the mass ratio of terpineol to anatase-titania nanoparticles was 4:1. A mesoporous TiO_2 film was deposited onto the compact TiO_2 blocking layer by spin coating the above paste at 3000 rpm for 40 s, followed by annealing at 500 ℃ for 30 min, and then cooling down to room temperature. Finally, CH_3NH_3I was synthesized by the method reported [1]. Fluorine -doped tin oxide (FTO) glasses (Pilkington), purchased from Yingkou Optimal Choice Trade CO., Ltd, were cleaned by ultrasonication with electronic cleaning fluid for 30 min. Next, the FTO glasses were cleaned with a mixed solution of ethanol and acetone (1:1) for 30 min, and then with isopropanol for 30 min. Finally, the cleaned FTO glasses were dried in an oven at room temperature.

2.4. Device fabrication

Perovskite precursors were obtained by mixing PbI_2, $PbCl_2$ and CH_3NH_3I (molar ratio 1:1:4) in N, N'-dimethylformamide (DMF). The $CH_3NH_3PbI_{3-x}Cl_x$ film was formed by spin coating the prepared solution onto the m -TiO_2 / c -TiO_2 / FTO substrate at 5000 rpm for 50s, then annealed at 70 ℃ for 30 min in ambient air, followed by 100 ℃ for 60 min in ambient air. A solution of PTB7 HTL was prepared by dissolving PTB7 in chlorobenzene(10mg/1 mL) with 7.5 μL of Li-TFSI / acetonitrile (170 mg / 1 mL) and 7.5 μL of t-Bp / acetonitrile (1mg / 1 mL) additives and without additives. The PTB7 HTL was spin-coated onto the prepared solution at 2000 rpm for 40 s, and the whole device underwent annealing at 80 ℃ for 30 min. Finally, a 100 nm thick silver counter electrode was deposited by thermal evaporation. As shown in figure 1a, the dot area of PSCs was 0.06 cm^2.

3. General principle of charge processes in PSCs

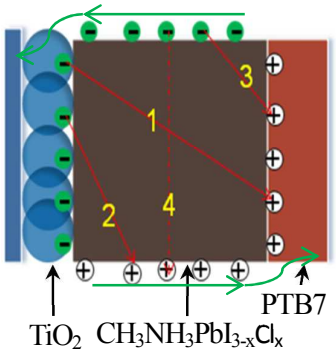

Figure 2 Schematic representation of carrier process in PSCs, where the green lines depict the ideal pathways of carrier transportation and the red arrows depict possible pathways of carrier recombination in PSCs.

The whole processes of carrier in PSCs ware presented in figure 2 and the red arrows illustrate the possible carrier recombination pathways according to the reported article [24]. When irradiated by light, the electrons and holes emerge and spread to the interfaces for extraction, then collecting by the both sides of the electrode. Due to the fact that more defect states exist in perovskite interface as the $CH_3NH_3PbI_{3-x}Cl_x$ films annealed at relatively low temperature, the plentiful carriers are accumulated and the velocity of charges extraction decrease, which indicates that the recombination of carriers easily occurs at the interfaces between different interfaces and the boundaries between grains of perovskite (figure 2). Accordingly, the interfacial defects can lead to the serious accumulation of carriers, and further bring about hysteresis of J-V performance. Therefore, the performance of PSCs is closely associated with the efficiency of excitons transmission, electrons (holes) extraction, and electrons (holes) transmission. Consequently, preparing absorber films that are uniform, smooth, pinhole-free, and have large amounts of crystallization and lower interfacial defect states plays a decisive role in overall device performance.

4. Results and discussion

The perovskite precursor was fabricated by above methods (section 2). Finally, the pin-free, pure crystalline $CH_3NH_3PbI_{3-x}Cl_x$ films were obtained. When these films acting as a light harvester and PTB7 serving as a HTL in PSCs, the device finally exhibited that 0.94 V of open circuit voltage (V_{oc}), 20.2 mA/cm^2 of short circuit density (J_{sc}), 70% of fill factor (FF), and 13.29% of power conversion efficiency (PCE) at forward scan direction

thereby yielding to 11.8% of average PCE.

Figure 3 a and b present scanning electron microscope (SEM) images, and Figure 3 c and d present atomic force microscope (AFM) images of $CH_3NH_3PbI_{3-x}Cl_x$ film interfaced to the c -TiO_2 and annealed in nitrogen (see Fig. 3 a and c) and ambient air (Fig. 3 b and d), respectively. As expected, a pinhole-free $CH_3NH_3PbI_{3-x}Cl_x$ film was obtained by annealing in both nitrogen and in ambient air; this is crucial to the final device performance insofar as it blocks direct contact between the TiO_2 and the HTL, thereby decreasing the leakage current (the pathway like 1 in Figure 2) and increasing FF. The grain sizes that arose from annealing in ambient air are larger than that of in nitrogen (Figures 3.a and b) and the surface roughness is approximately same for both (Figures 3.c and d). Bigger grains indicate that there exist fewer grain boundaries and then a lower density of interfacial states.

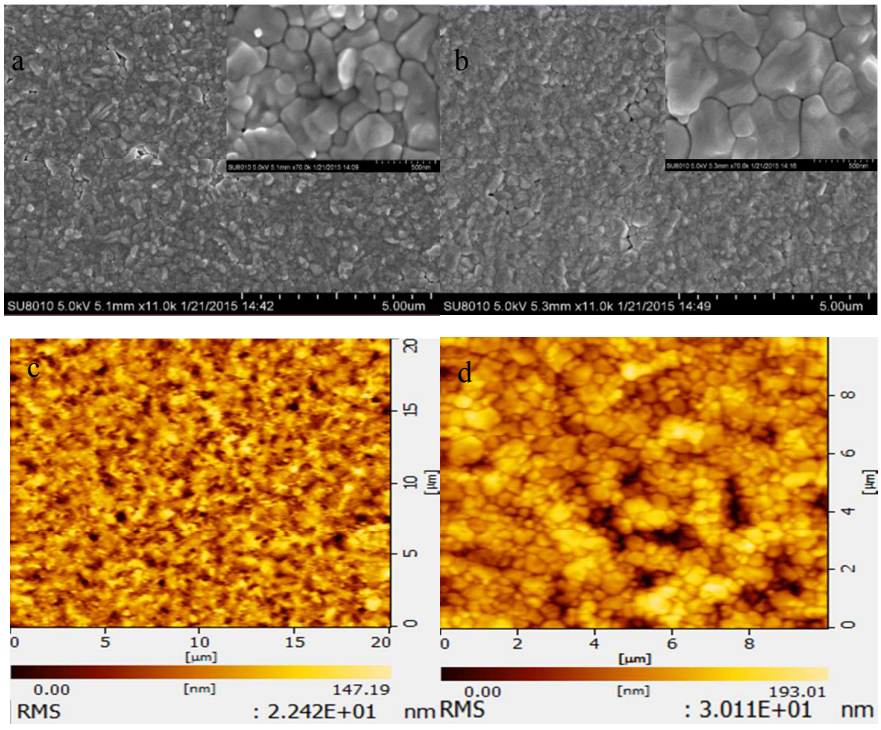

Figure 3 SEM images ((a), (b)) and AFM images ((c), (d)) of the $CH_3NH_3PbI_{3-x}Cl_x$ films annealed in nitrogen condition ((a), (c)) and in ambient air condition ((b), (d)), respectively. The larger amplification SEM images of $CH_3NH_3PbI_{3-x}Cl_x$ films are also inserted in figure 3.a and figure 3.b as insets.

Meanwhile, when the $CH_3NH_3PbI_{3-x}Cl_x$ was annealed in ambient air, adjacent grains not only displayed dense integration, but exhibited better crystallization. Although the fact is that a small amount of moisture can

result in the decomposition of perovskite and the appearance of residual PbI_2, which is due to the fact that the organic compound CH_3NH_3I easily absorbs moisture from the ambient air and change the forming process of perovskite films [15, 16], some studies have demonstrated that such decomposition often appears in grain boundaries, which can play the role of passivation and alleviate the defect states, thereby better connecting adjacent grains [25,26]. All these factors make it possible to greatly reduce the carrier recombination that occurs in the grain boundaries, thereby improving current density.

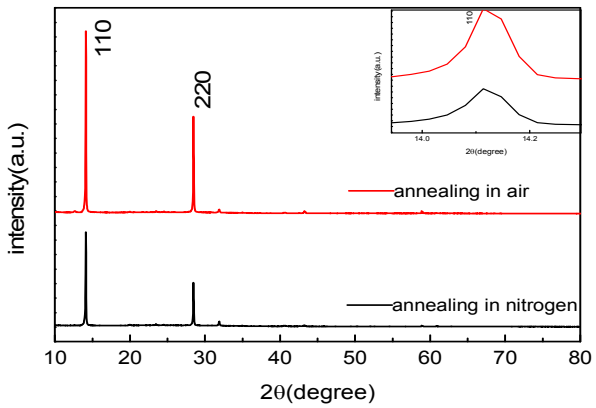

Figure 4 the image of XRD of $CH_3NH_3PbI_{3-x}Cl_x$ films, where the red line depicts film annealed in ambient air atmosphere, and the black line depicts film annealed in nitrogen. Inset shows the amplification image of XRD diffraction peak at 14.17° corresponding to the $CH_3NH_3PbI_{3-x}Cl_x$ films annealing in air (red) and in nitrogen (black), respectively.

In order to verify these suppositions, X-ray diffraction (XRD) measurements were taken. As figure 4 show, two prevalent XRD diffraction peaks at 14.17° and 28.51° appear, which is indicative of the performed perovskite phases of (110) and (220) arising from the tetragonal $CH_3NH_3PbI_{3-x}Cl_x$ crystal structure. As the inset in figure 4 shows, the (110) diffraction peak in air atmosphere appears to be narrower than that in nitrogen when investigated by amplification, which implies the crystal size of the perovskite crystallites prepared in air atmosphere are much larger than that prepared in nitrogen with all other conditions being the same, which is consistent with the results observed by SEM. It is also remarkable that relative pure perovskite phase was obtain even we prepared the perovskite film in ambient air, which would decrease the defect states in perovskite inner materials.

After achieving a pinhole-free, high -quality perovskite film, we then deposited the organic polymer PTB7 on the absorber as the HTL and fabricated the photovoltaic device. Furthermore, we compared the performance of this device with that of solar cells with different HTLs, including PTB7, P3HT, PCDTBT and Spiro-OMeTAD. Fortunately, the results show that the device with PTB7 can exhibit considerable performance among the devices fabricated with different HTLs (see Figure 5). To the best of our knowledge, this is the first time that PTB7 has been used as a HTL in efficient PSCs. The relevant Photovoltaic parameters derived from J-V measurements corresponding to Figure 5 are summarized in table 1. Evidently, the PTB7-based PSCs are superior to other HTLs-based PSCs, including the improved V_{oc} and FF values (see figure 5 and table 1).

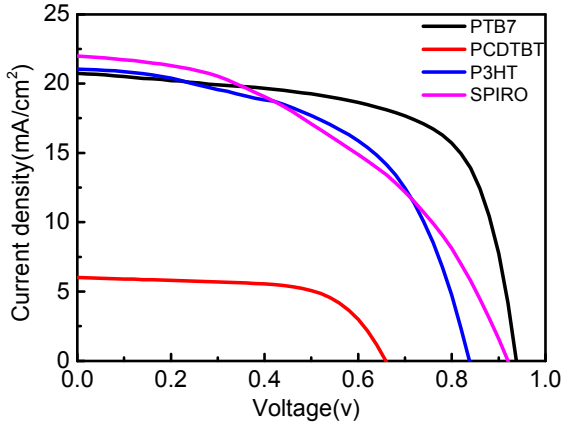

Figure 5 J-V measurements of the devices with FTO / c-TiO_2 / m-TiO_2 / $CH_3NH_3PbI_{3-x}Cl_x$ / diverse HTLs / Silver (under identical preparation conditions), where the black line corresponds to PTB7; the red line corresponds to PCDTBT; the blue line corresponds to P3HT; the purple line corresponds to Spiro-OMeTAD.

Table 1 Photovoltaic parameters derived from J-V measurements corresponding to Figure 5

HTL	J_{sc} (mA/cm^2)	V_{oc} (V)	FF	PCE (%)	Series resistance(Ω)	Shunt resistance(Ω)
PTB7	20.7	0.94	0.65	12.65	4.8	667
PCDTBT	6.0	0.66	0.64	2.53	16.4	825
P3HT	21.0	0.84	0.54	9.53	7.6	203
Spiro-OMeTAD	22.0	0.92	0.44	8.91	12.6	206

We suggest that the main advantages of PTB7 can be attributed to its excellent conductivity. This is demonstrated by the results of the conductivity test, presented in Table 2. When added to LiTFSI and t-Bp, PTB7 exhibits better conductivity, which can not only decrease the series resistance in PSCs (Table 1), but increase the lateral collection of charges, and thus improve the FF in PSCs. By the further process optimization, the FF of PSCs can reach as high as 70%.

Table 2 the measurements of conductivity of diverse HTLs

HTL	Conductivity (S/cm)
PTB7(additive and annealing)	9.5×10^{-5}
P3HT(additive and annealing)	3.0×10^{-6}
Spiro(additive and annealing)	2.0×10^{-6}

Moreover, the minimal influence that spin coating PTB7 has on the perovskite film significantly also contributes to the device's impressive performance, which could be demonstrated by the test of transmittance and absorption spectra (see figure 6). Ultraviolet–visible (UV-vis) spectra were recorded for $CH_3NH_3PbI_{3-x}Cl_x$ before and after spin-coating with PTB7 (Figure 6) and the incident light irradiate from the membrane surface. It can be clearly seen that the absorption capacity was enhanced after spinning PTB7 (see figure 6.c), especially in the wavelength range from 500 nm to 760 nm, which has inferior absorption for perovskite films. This can be attributed to the influence of the PTB7 absorbing more extra photons because of its effective optical absorption coefficient compared with the sample before spin–coating PTB7, thereby ensuring a sufficient photon absorption. The most important matter is that the absorption trend of $CH_3NH_3PbI_{3-x}Cl_x$ does not distinctly change with the addition of PTB7, which could indicate that the PTB7 does not degrade the quality of the perovskite film. If the $CH_3NH_3PbI_{3-x}Cl_x$ films have been destroyed with the coating of PTB7, the absorption spectra will present the distinctive unlike absorbing trend of $CH_3NH_3PbI_{3-x}Cl_x$, especially in long wavelengths. Consequently, these results powerfully indicate that after coating PTB7, there is little impact on the underlying $CH_3NH_3PbI_{3-x}Cl_x$ and the absorption of visible light in the device is improved. By incorporating the PTB7 as an HTL, the whole device can absorb sunlight over the entire visible range, which is crucial to the improvement of current density.

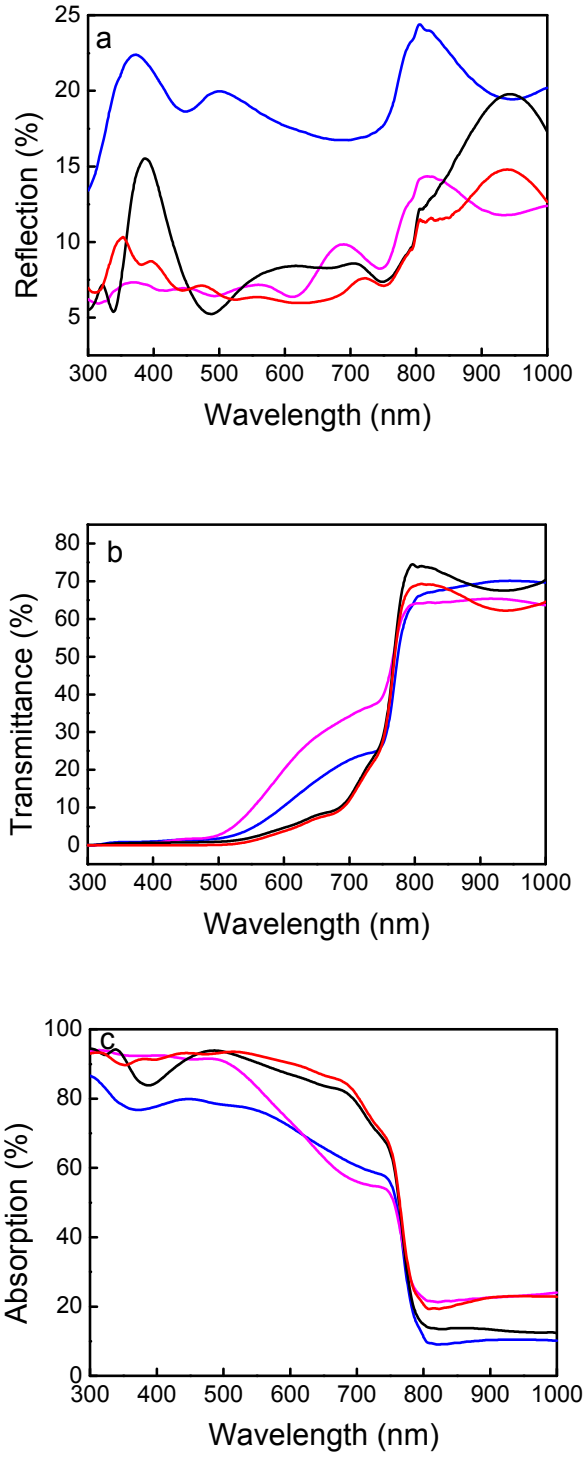

Figure 6 The spectrums of reflection, transparent and absorption are shown in (a), (b), (c), respectively, where the black line stands for $CH_3NH_3PbI_{3-x}Cl_x$ coated PTB7 and annealed in nitrogen, the red line stands for $CH_3NH_3PbI_{3-x}Cl_x$ coated PTB7 and annealed in ambient air, the blue line stands for $CH_3NH_3PbI_{3-x}Cl_x$ annealed in nitrogen, the purple line stands for $CH_3NH_3PbI_{3-x}Cl_x$ annealed in ambient air.

Finally, it is widely known that the HTL of spiro-OMeTAD often requires the doping of LiTFSI and

t-Bp in PSCs in order to enhance conductivity, and that the crystallization of HTL could be also enhanced by post-annealing. [27] Accordingly, in order to further enhance the performance of PSCs with PTB7, we explored the influence of doping and post-annealing on the overall device performance. Figure 7 depicts the J-V characteristics. The photovoltaic parameters of the corresponding curves are shown in Table 3. It can be noted that series resistance greatly decrease from 12.04 to 3.2 with the addition of additives and the introduction of post-annealing process (while other conditions are left unchanged). Accordingly, J_{sc} exhibit stable improvement with the decrease of the series resistance, which is caused by the enhancement of holes collection of HTL. It is assumed that in the process of post-annealing, the organic molecule PTB7 adjusts its orientation to form an optimal contact with the perovskite in spite of presenting the amorphous, thereby decreasing the contact resistance, and improving the FF. As for the role of the two additives, it is believed that they can enhance the conductivity of PTB7, which constitutes their function in spiro-MoTAD.

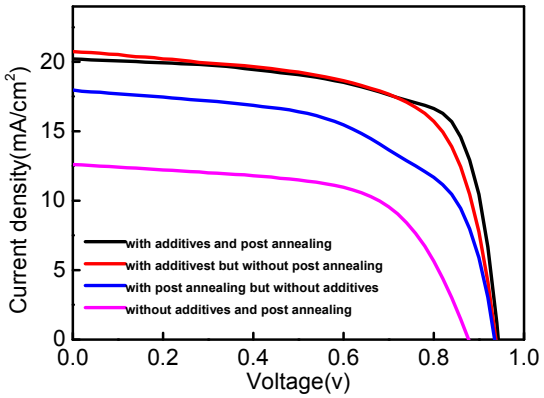

Figure 7 the J-V characteristics of PSCs with construction of FTO / c-TiO2 / m-TiO2 / $CH_3NH_3PbI_{3-x}Cl_x$ / PTB7 / Silver, where the purple line depicts device without additives and post annealing process, the blue line depicts device without additives but with post annealing process, the red line depicts device with additives but without annealing, the black line depicts device with additives and annealing.

Table 3 Photovoltaic parameters derived from J-V measurements corresponding to Figure 7

Preparation condition	J_{sc} (mA/cm^2)	V_{oc} (V)	FF	PCE (%)	Series resistance(Ω)	Shunt resistance(Ω)
PTB7(dopant and annealing)	20.2	0.94	0.7	13.29	3.2	655
PTB7(dopant)	20.7	0.94	0.63	12.7	4.82	667
PTB7(annealing)	18	0.93	0.57	9.57	5.0	230
PTB7	12.6	0.87	0.62	6.8	12.04	541

5. Conclusions

In summary, a new HTL composed of PTB7 was adopted for manufacturing efficient $CH_3NH_3PbI_{3-x}Cl_x$ PSCs and the whole fabrication processes (except for the metal electrode) conducted in ambient air were achieved. The PTB7 not only possesses higher conductivity but has proper band alignment with $CH_3NH_3PbI_{3-x}Cl_x$ perovskite material. Meanwhile, the property of PTB7 is also easily modified by plain post-annealing process, or certain additives to PTB7, along with minimal influence of PTB7 on the under perovskite film. By the various comparative tests, we believe that PTB7 has a lower resistance for carrier transfer and better interface contact characteristics, which facilitate the extraction and transportation of hole when interacted with $CH_3NH_3PbI_{3-x}Cl_x$ film. We will continue working hard to explore more evidences to support these views. In a word, these findings demonstrate that a new PTB7 HTL was introduced to the PSCs and many merits were investigated. The results presented here and the overall fabrication method represent a helpful new approach for fabricating highly efficient perovskite -based photovoltaic devices.

Acknowledgements

This work was supported by National Natural Science Foundation of China (Grant No. 61377031), the National Natural Science Foundation of China（No.61404073）and the Specialized Research Fund for the Doctoral Program of Higher Education (No. 20120031120044).

References

[1] Kojima A, Teshima K, Shirai Y, et al. Organometal halide perovskites as visible-light sensitizers for photovoltaic cells[J]. Journal of the American Chemical Society, 2009, 131(17): 6050-6051.

[2] Stranks S D, Eperon G E, Grancini G, et al. Electron-hole diffusion lengths exceeding 1 micrometer in an organometal trihalide perovskite absorber[J]. Science, 2013, 342(6156): 341-344.

[3] Lee M M, Teuscher J, Miyasaka T, et al. Efficient hybrid solar cells based on

meso-superstructured organometal halide perovskites[J]. Science, 2012, 338(6107): 643-647.

[4] Wang J, Qin M, Tao H, et al. Performance enhancement of perovskite solar cells with Mg-doped TiO2 compact film as the hole-blocking layer[J]. Applied Physics Letters, 2015, 106(12): 121104.

[5] Im J H, Lee C R, Lee J W, et al. 6.5% efficient perovskite quantum-dot-sensitized solar cell[J]. Nanoscale, 2011, 3(10): 4088-4093.

[6] Ball J M, Lee M M, Hey A, et al. Low-temperature processed meso-superstructured to thin-film perovskite solar cells[J]. Energy & Environmental Science, 2013, 6(6): 1739-1743.

[7] Burschka J, Pellet N, Moon S J, et al. Sequential deposition as a route to high-performance perovskite-sensitized solar cells[J]. Nature, 2013, 499(7458): 316-319.

[8] Liu M, Johnston M B, Snaith H J. Efficient planar heterojunction perovskite solar cells by vapour deposition[J]. Nature, 2013, 501(7467): 395-398.

[9] Liu D, Kelly T L. Perovskite solar cells with a planar heterojunction structure prepared using room-temperature solution processing techniques[J]. Nature Photonics, 2014, 8(2): 133-138.

[10] Jeon N J, Noh J H, Yang W S, et al. Compositional engineering of perovskite materials for high-performance solar cells[J]. Nature, 2015, 517(7535): 476-480.

[11] Kuang, C., Tang, G., Jiu, T., Yang, H., Liu, H., Li, B., & Li, Y. (2015). Highly Efficient Electron Transport Obtained by Doping PCBM with Graphdiyne in Planar-Heterojunction Perovskite Solar Cells. Nano letters.

[12] MingáLau, Woon. "Highly efficient fullerene/perovskite planar heterojunction solar cells via cathode modification with an amino-functionalized polymer interlayer." Journal of

Materials Chemistry A 2.46 (2014): 19598-19603.

[13] Xiao M, Huang F, Huang W, et al. A fast deposition‐crystallization procedure for highly efficient lead iodide perovskite thin‐film solar cells[J]. Angewandte Chemie, 2014, 126(37): 10056-10061.

[14] Wang D, Liu Z, Zhou Z, et al. Reproducible One-Step Fabrication of Compact M $APbI_{3-x}Cl_x$ Thin Films Derived from Mixed-Lead-Halide Precursors [J]. Chemistry of Materials, 2014, 26(24): 7145-7150.

[15] You J, Yang Y M, Hong Z, et al. Moisture assisted perovskite film growth for high performance solar cells[J]. Applied Physics Letters, 2014, 105(18): 183902.

[16] Zhou H, Chen Q, Li G, et al. Interface engineering of highly efficient perovskite s olar cells[J]. Science, 2014, 345(6196): 542-546.

[17] Dkhissi Y, Huang F, Rubanov S, et al. Low temperature processing of flexible planar perovskite solar cells with efficiency over 10%[J]. Journal of Power Sources, 2015, 278: 325-331.

[18] Lin Q, Armin A, Nagiri R C R, et al. Electro-optics of perovskite solar cells[J]. Nature Photonics, 2014.

[19] Kim J H, Kim D, Shin H W, et al. Planar CH3NH3PbI3 Perovskite Solar Cells with Constant 17.2% Average Power Conversion Efficiency Irrespective of the Scan Rate Jin Hyuck Heo, Dae Ho Song, Hye Ji Han, Seong Yeon Kim[J].

[20] Qin P, Tetreault N, Dar M I, et al. A novel oligomer as a hole transporting material for efficient perovskite solar cells [J]. Advanced Energy Materials , 2014.

[21] Heo J H, Im S H. CH3NH3PbI3/poly‐3‐hexylthiophen perovskite mesoscopic solar cells: Performance enhancement by Li‐assisted hole conduction [J]. physica status solidi (RRL)-Rapid Research Letters, 2014, 8(10): 816-821.

[22] Ryu S, Noh J H, Jeon N J, et al. Voltage output of efficient perovskite solar cells with high open-circuit voltage and fill factor[J]. Energy Environ. Sci., 2014, 7(8): 2614-2618.

[23] Christians J A, Fung R C M, Kamat P V. An inorganic hole conductor for organo-lead halide perovskite solar cells. Improved hole conductivity with copper iodide [J]. Journal of the American Chemical Society, 2013, 136(2): 758-764.

[24] Marchioro A, Teuscher J, Friedrich D, et al. Unravelling the mechanism of photoinduced charge transfer processes in lead iodide perovskite solar cells[J]. Nature photonics, 2014, 8(3): 250-255.

[25] Chen Q, Zhou H, Song T B, et al. Controllable self-induced passivation of hybrid lead iodide perovskites toward high performance solar cells[J]. Nano letters, 2014, 14(7): 4158-4163.

[26] Supasai T, Rujisamphan N, Ullrich K, et al. Formation of a passivating $CH_3NH_3PbI_3/PbI_2$ interface during moderate heating of $CH_3NH_3PbI_3$ layers[J]. Applied Physics Letters, 2013, 103(18): 183906.

[27] Fang Y, Wang X, Wang Q, et al. Impact of annealing on spiro-OMeTAD and corresponding solid‐state dye sensitized solar cells[J]. physica status solidi (a), 2014, 211(12): 2809-2816.